Low-energy Neutrino-Nucleus Cross Sections

Natalie Jachowicz

Ghent University, Department of Physics and Astronomy, Proeftuinstraat 86, B-9000 Gent, Belgium

DOI: http://dx.doi.org/10.3204/DESY-PROC-2011-03/jachowicz

We present an overview of neutrino-nucleus scattering at low energies and highlight the aspects of the study of these interactions important for supernova physics.

1 Introduction

Neutrinos are important for a type II supernova explosion in several ways. On one hand, neutrino interactions and the related energy transfers play a crucial role in the explosion dynamics and nucleosynthesis. On the other hand, the terrestrial detection of supernova neutrinos can provide a broad variety of information [1] about the neutrinos and their interactions, and about the supernova process itself. The arrival times of the neutrinos are related to their mass and can moreover hint at the fate of the star. Several reactions provide directional information, important for optical telescopes awaiting the photons in the wake of the supernova neutrino flux. The energy of the neutrinos can be inferred from the energy of the decay products. It indicates the decoupling site of the neutrinos and the temperature there. As mu and tau supernova-neutrinos do not have enough energy to produce a massive lepton in a charged-current reaction, the flavor of the arriving neutrinos can be inferred from the frequency differences between the occurrence of neutral and charge-exchange processes. Whether a neutrino or an antineutrino entered the detector can be determined by looking at the charge of the outgoing lepton for electron (anti)neutrinos or by examining the spin of the outgoing nucleon in neutral-current nucleon knockout off nuclei. When the signal in the detector is accurately resolved, the observed neutrino energies and flavors can help to disentangle the mixing scheme induced by oscillations [2, 3].

Nuclei have relatively large cross sections for neutrino reactions and are energy-sensitive in the range of interest, several particle-emission thresholds opening up with increasing incoming neutrino energies. This makes nuclear targets important as detecting material. Galactic supernova neutrinos could be detected by existing and proposed supernova neutrino detectors such as SNO [4], SuperKamiokande [5], KamLAND [1], LVD [6], MiniBooNe [7], OMNIS [8], LAND [9]. Favored detection nuclei are ^{12}C, ^{16}O, ^{56}Fe, ^{208}Pb, and deuterium. However, the signal in the detector can only be interpreted as well as the relevant neutrino-nucleus cross sections are understood. For most nuclei very little experimental neutrino data exists in the relevant energy region. This is due to the very small cross sections for weak interaction processes, and an additional limitation is caused by the fact that monochromatic neutrino beams are not available [10, 11]. This has as a consequence that for most applications one has to rely on theoretical

predictions, with their related uncertainties and model dependencies.

2 Modeling neutrino-nucleus interactions at low energies

The study of the atomic nucleus faces particular problems : generally, the atomic nucleus is a mesoscopic system, on the one hand containing too much particles to allow few-body techniques to be effective and on the other hand containing too few nucleons to enable a statistical approach of the problem. In the tens-of-MeV energy range important for supernova neutrinos, cross sections are very sensitive to nuclear structure effects.

The main methods to study neutrino scattering off nuclei at supernova-neutrino energies are the Shell Model (SM) and the Random Phase Approximation (RPA). In the former, the description of the nucleus is based on a full diagonalization of a effective interaction in a limited model space. In recent years, the shell model has been used successfully to study various weak interactions of interest to nuclear astrophysics [12]. The main disadvantage of the shell model approach is the dimension of the matrices to be diagonalized, rapidly growing with increasing model sizes.

Confronted with this drawback, a number of approximations has been designed, focusing on various aspect of the problem. Next to the Hartree-Fock approximation, considering only single-particle properties of the problem, more elaborate techniques as e.g. the RPA were developed. Contrary to mean-field descriptions were a nucleon experiences the presence of the others only through the mean-field generated by their mutual interactions, the random phase approximation allows correlations to be present even in the ground state of the nuclear system and additionally allows the particles to interact by means of the residual two-body force. The random phase approximation goes one step beyond this zeroth-order mean-field approach and describes a nuclear state as the coherent superposition of particle-hole contributions.

$$|\Psi_{RPA}\rangle = \sum_c \left\{ X_{(\Psi,C)} \ \left|ph^{-1}\right\rangle \ - \ Y_{(\Psi,C)} \ \left|hp^{-1}\right\rangle \right\}. \tag{1}$$

The summation index C stands for all quantum numbers defining a reaction channel unambiguously :

$$C = \{n_h, l_h, j_h, m_h, \varepsilon_h; l_p, j_p, m_p, \tau_z\}, \tag{2}$$

where the indices p and h indicate whether the considered quantum numbers relate to the particle or the hole state, ε_h denotes the binding-energy of the hole state and τ_z defines the isospin character of the particle-hole pair. General excited states are obtained as linear combinations of these particle-hole configurations. As the RPA approach describes nuclear excitations as the coherent superposition of individual particle-hole states out of a correlated ground state, this approach allows to account for some of the collectivity present in the nucleus. In standard RPA calculations this leads to a discrete spectrum, with several variations in the approach [13, 14, 15] in use.

In this contribution, the cross section results are illustrated using a Continuum Random Phase Approximation (CRPA), based on a Green's function approach [16, 17, 18]. The unperturbed wave-functions are generated using either a Woods-Saxon potential or a HF-calculation using a Skyrme force. The latter approach makes self-consistent HF-RPA calculations possible.

The differential cross-section for scattering of an incoming neutrino with energy ε_i is given by

$$\left(\frac{d^2\sigma_{i\to f}}{d\Omega d\omega}\right)_{\substack{\nu\\ \bar{\nu}}} = \frac{G^2\varepsilon_f^2}{\pi}\,\frac{2\cos^2\left(\frac{\theta}{2}\right)}{2J_i+1}\left[\sum_{J=0}^{\infty}\sigma_{CL}^J + \sum_{J=1}^{\infty}\sigma_T^J\right], \tag{3}$$

with

$$\sigma_{CL}^J = \left|\left\langle J_f \left|\left| \widehat{\mathcal{M}}_J(\kappa) + \frac{\omega}{|\vec{q}|}\widehat{\mathcal{L}}_J(\kappa)\right|\right| J_i\right\rangle\right|^2, \tag{4}$$

$$\begin{aligned}\sigma_T^J \;=\; & \left(-\frac{q_\mu^2}{2\,|\vec{q}|^2} + \tan^2\left(\frac{\theta}{2}\right)\right)\left[\left|\left\langle J_f\left|\left|\widehat{\mathcal{T}}_J^{mag}(\kappa)\right|\right| J_i\right\rangle\right|^2 + \left|\left\langle J_f\left|\left|\widehat{\mathcal{T}}_J^{el}(\kappa)\right|\right| J_i\right\rangle\right|^2\right] \\ & \mp \tan\left(\frac{\theta}{2}\right)\sqrt{-\frac{q_\mu^2}{|\vec{q}|^2} + \tan^2\left(\frac{\theta}{2}\right)}\;\left[2\Re\left(\left\langle J_f\left|\left|\widehat{\mathcal{T}}_J^{mag}(\kappa)\right|\right| J_i\right\rangle\left\langle J_f\left|\left|\widehat{\mathcal{T}}_J^{el}(\kappa)\right|\right| J_i\right\rangle^*\right)\right],\end{aligned} \tag{5}$$

where $\widehat{\mathcal{M}}_J$ and $\widehat{\mathcal{L}}_J$ are the Coulomb and longitudinal multipole operators, $\widehat{\mathcal{T}}_J^{mag}$ and $\widehat{\mathcal{T}}_J^{el}$ the transverse multipole operators. θ is the scattering angle of the lepton. For each multipole transition J^π only one part -vector or axial vector- of an operator is contributing. From the expression (3) it is clear that J=0 transitions are suppressed due to the lack of a transverse contribution in these channels. Still, neutrinos are able to excite 0^- states in nuclei, while electrons cannot. The second and third part of the expression show that there is interference between the Coulomb and the longitudinal (CL) terms and between both transverse contributions, but not between transverse and CL terms. The only difference between neutrino and antineutrino cross-sections is in the opposite sign of the transverse interference part. From the angular dependence of the kinematic factors, it is clear that for backwards $\theta = \pi$ scattering only transverse terms contribute, while for $\theta = 0$ CL-contributions dominate.

For charged current neutrino scattering reactions, the outgoing particle is a charged lepton. In this case, the outgoing particle has to be described by the scattering solutions in the Coulomb potential generated by the final nucleus. For the applications considered here, this can be done in an effective way introducing the Fermi function. The cross-section is then multiplied by the square of the ratio between the correct scattering solution and a plane wave for a point charge Z', evaluated at the origin.

For many applications, the direction of the outgoing lepton is irrelevant and the differential cross-section has to be integrated over the scattering angle $\Omega(\theta, \phi)$. Considering a process where the incoming neutrino energies are distributed according to a spectrum, the cross-section (3) has to be folded with this energy distribution. The total scattering cross-section is obtained by performing an integration of (3) over the excitation energies ω and summing over the different multipole contributions.

3 Cross sections

Neutrino scattering potentially constitutes a rich source of information on nuclear structure and weak interaction characteristics. But notwithstanding the experimental efforts, the extraction of information out of scattering reactions is very difficult, due to the very small interaction cross-sections. The importance of neutrinos in a variety of astrophysical situations therefore

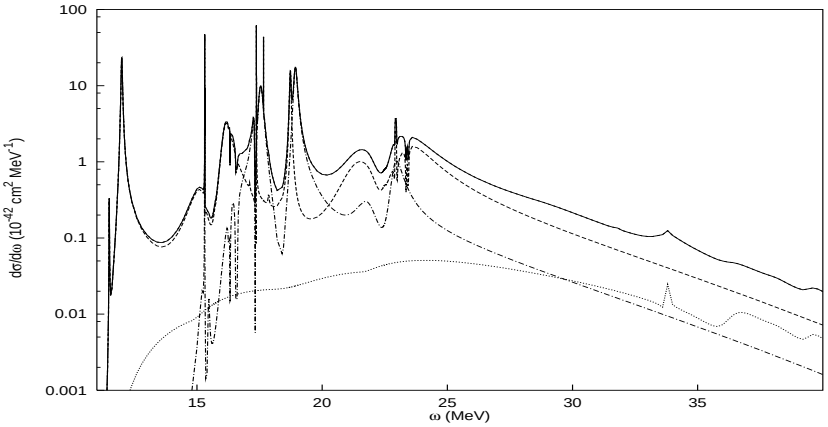

Figure 1: Cross-section for the neutral current reaction $^{16}O + \nu_{50\,MeV} \rightarrow {}^{16}O^* + \nu'$ (full line) and its dominant multipole contributions. $J^\pi = 1^-$ (dashed line), $J^\pi = 1^+$ (dashed-dotted) and $J^\pi = 2^-$ (dotted line). The total cross-section includes multipoles up to J=4. The single-particle wave-functions and energies were obtained with a Hartree-Fock calculation, as residual interaction the SkE2 parameterization was used.

represents an important additional motivation for the study of neutrino-nucleus scattering reactions.

In this section, the main characteristics of neutrino-nucleus scattering at supernova-neutrino energies are discussed using the example of neutral-current scattering of 50 MeV neutrinos off ^{16}O.

Figure 1 shows the differential cross-section for this reaction as a function of the excitation energy ω of the nucleus, and the most important multipole contributions. The differential neutrino scattering cross-sections are of the order of 10^{-42} cm^2 per MeV. The figure clearly illustrates that at energies below 20 MeV, the cross-section spectrum is sharply peaked. These peaks are related to excitations with a strong single-particle character. The resonances are however very narrow and therefore do not absorb all transition strength. At excitation energies between 20 and 25 MeV, the broad resonance structure of the giant dipole resonance shows up. For excitation energies above approximately 30 MeV the cross-section decreases almost purely quadratically as a function of the excitation energy of the nuclear system. This agrees with the energy dependence of equation (3) which shows the cross-section to be proportional to the square of the outgoing lepton energy $\frac{d\sigma}{d\omega} \sim (\varepsilon_f)^2$. This effect furthermore results in the smooth and soft broadening of the resonances for higher values of the energy of the lepton projectile.

In the calculation, multipoles up to J=4 were taken into account. Contributions of higher order multipole excitations were found to be very small at the considered energies. The J=5 transitions are suppressed by almost 5 orders of magnitude and as a consequence have negligible influence on the total cross-section. The smooth behavior of these contributions furthermore assures that the shape of the resonance structure in the excitation spectrum is not affected by the higher order multipole transitions.

The J=1 excitations are prominent, with a clear dominance of the J=1$^-$ electric dipole transition in the giant resonance region. Next to higher order multipole transitions J=3 and

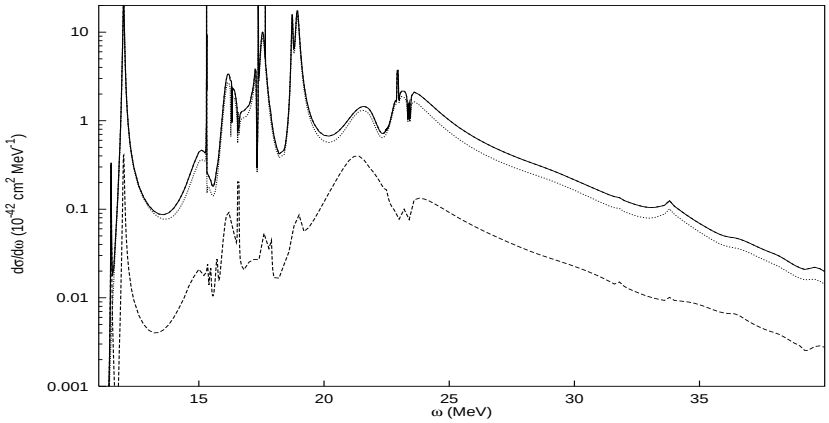

Figure 2: Comparison between the vector (dashed) and the axial vector (dotted line) contribution to the reaction $^{16}O(\nu,\nu')^{16}O^*$. The total differential cross-section is shown by the full curve.

J=4, also J=0 excitations are suppressed. This is due to the fact that only Coulomb and longitudinal terms contribute to these channels. But still, some clear 0^- resonances show up in the differential cross-sections. In general, negative parity transitions are clearly dominating the positive parity contributions. For higher excitation energies, the relative importance of higher order multipoles increases.

Figure 2 carries out a comparison between the contribution of the axial and the axial vector part of the hadronic current to the total cross-section. The axial vector current is clearly more sensitive to the weak neutrino probes. The vector contribution is suppressed by more than one order of magnitude. The splitting of the cross-section in a vector and an axial vector part excludes the interference contribution. This explains the discrepancy between the sum of both curves in figure 2 and the total cross-section.

Due to the fact that the axial vector current is completely isovector, isovector excitations will dominate isoscalar ones, as figure 4 indeed illustrates. The reason for the large suppression of the isoscalar excitations is twofold : not only is the axial vector current not contributing to isoscalar transitions, but due to the $\sin^2\theta_W$-factor the isoscalar form factors are considerably smaller than the vector ones as well. A further consequence of this isovector dominance is the large isovector contribution to the resonance at 23.6 MeV, a dominance that is clearly related to the axial vector character of this excitation (figure 2). The figure furthermore shows that, due to the repulsive character of the interaction in the isovector channels, isovector excitations are pushed towards higher energies compared to isoscalar states.

According to equation (3) it is the interference contribution that is responsible for the difference in the nuclear response to neutrino and antineutrino perturbations. The sign of the interference term determines which cross-section will be dominant. Figure 3 illustrates that generally neutrino cross-sections are slightly larger than antineutrino cross-sections. Only round 23 MeV, the interference term changes sign and antineutrino excitations become more important.

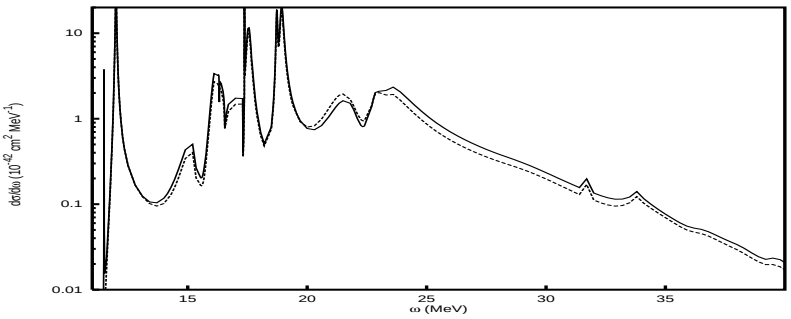

Figure 3: Cross-section for neutral current neutrino (full line) and antineutrino (dashed) scattering reactions off oxygen 16.

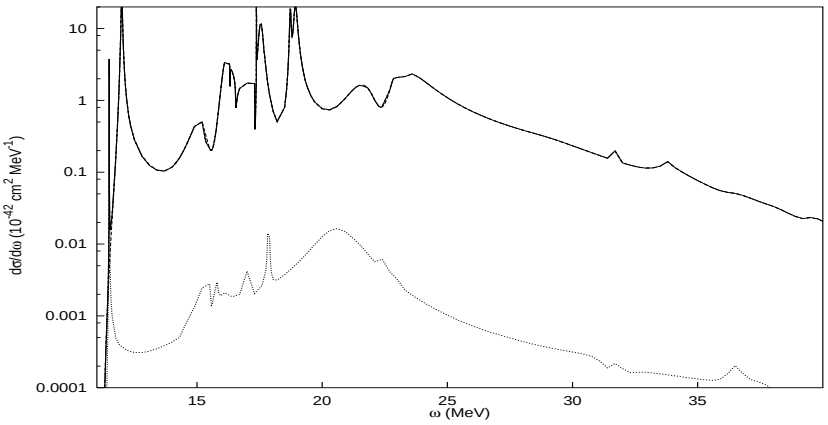

Figure 4: Comparison between the isovector (dashed line) and the isoscalar (dotted) contribution to the reaction $^{16}O(\nu,\nu')^{16}O^*$. The isovector curve almost coincides with the total cross-section.

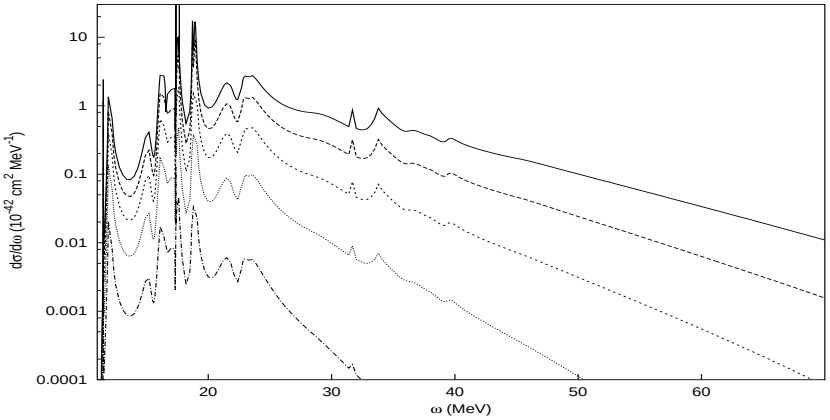

Figure 5: Differential cross-section for the neutral current reaction $^{16}O + \nu_{FD} \rightarrow {}^{16}O^* + \nu'$, averaged over neutrinos and antineutrinos and over a Fermi-Dirac distribution with temperature T and vanishing chemical potential. T=12 MeV (full line) ; T=10 MeV (dashed) ; T=8 MeV (shortdashed) ; T=6 MeV (dotted) and T=4 MeV (dashed-dotted).

4 Influence of the energy distribution

In order to obtain information about the interactions of supernova neutrinos, the cross sections have to be folded with the appropriate energy spectrum. Figure 6 shows that the folded cross section is strongly dependent on the temperature or average energy of the distribution. Traditionally, supernova-neutrino energy-distributions were parametrized using Fermi-Dirac distributions. The spectra are however not purely thermal, as the decoupling sites of the neutrinos are influenced by their flavor and energy, leading to the use of "effective temperatures" and "effective chemical potentials" in these distributions. Recent calculations showed that descriptions of a supernova neutrino spectrum are provided by a power-law distribution [19]:

$$n_{SN[\langle\varepsilon\rangle,\alpha]}(\varepsilon) = \left(\frac{\varepsilon}{\langle\varepsilon\rangle}\right)^{\alpha} e^{-(\alpha+1)\frac{\varepsilon}{\langle\varepsilon\rangle}}, \tag{6}$$

where $\langle\varepsilon\rangle$ and α represent the average energy and the width of the spectrum respectively. The average neutrino energy $\langle\varepsilon\rangle$ is related to the temperature at the decoupling site, and the effect of α is equivalent to that of the introduction of the effective chemical potential in the Fermi-Dirac distribution. Neutrino-nucleus reaction cross sections depend on the square of the incoming energy, thus rising very fast with neutrino energies. Hence, the folded cross sections reach their maximum at much higher energy values than the supernova-neutrino energy-spectrum does, as illustrated in figure 6. Typically even neutrinos with energies more than twice the average energy of the distribution make sizable contributions to the folded cross section, and integrated cross sections only converge at energies above 60 MeV [20]. This makes the high-energy tail of the spectra very important for the determination of the nuclear response.

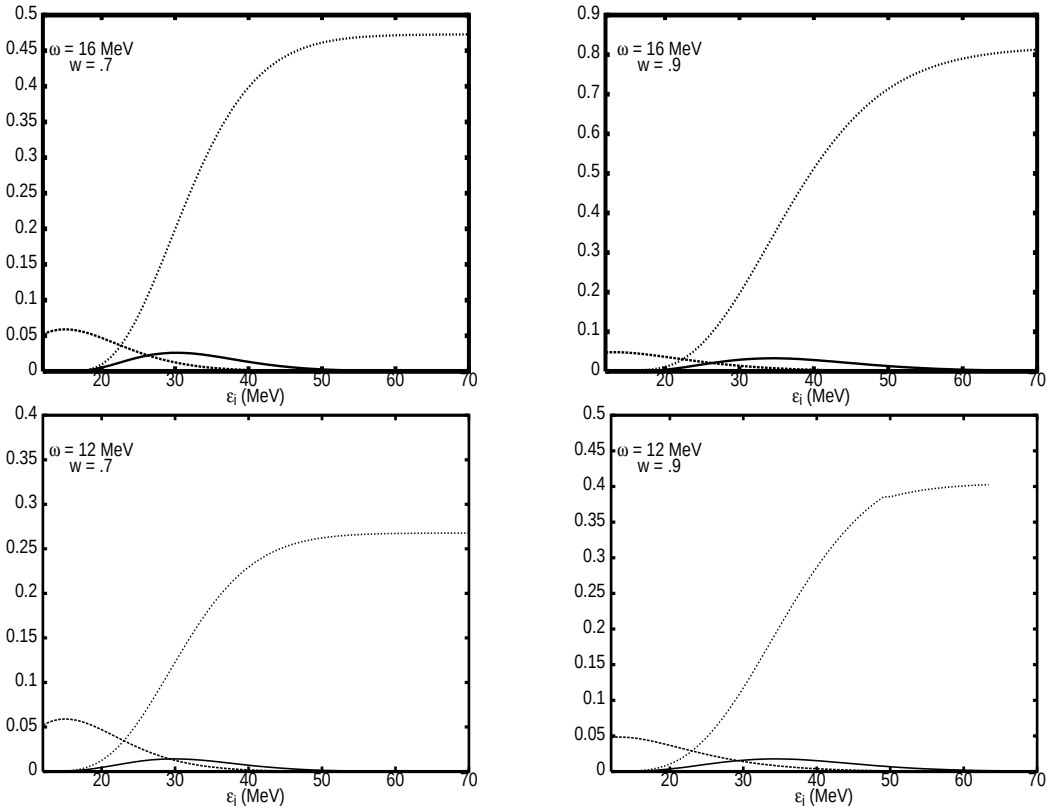

Figure 6: Influence of the supernova-neutrino energy-distribution on the folded cross section for different spectra and excitation energies of the nucleus: energy spectrum (dotted), cross section (dashed), folded cross section (full line).

5 Neutrino interactions at a low-energy beta-beam facility

Beta beams, which are neutrino beams produced by the beta decay of nuclei that have been accelerated to high gamma factor, were original proposed for high energy applications, such as the measurement of the third neutrino mixing angle θ_{13} [21]. Volpe [22, 23, 24] suggested that a beta beam run at lower gamma factor, would be useful for neutrino measurements in the tens of MeV range. The flexibility these beta-beam facilities offer [25], combined with the fact that beta-beam neutrino energies overlap with supernova-neutrino energies, allow one to construct 'synthetic' spectra that approximate an incoming supernova-neutrino energy-distribution. It can be shown that fitting 'synthetic' spectra, constructed by taking linear combinations of beta-beam spectra, to the original supernova-neutrino spectra reproduces the folded differential cross sections very accurately [26, 27]. Comparing the response in a terrestrial detector to these synthetic responses provides a direct way to determine the main parameters of the supernova-neutrino energy-distribution. Using these constructed spectra we are able to reproduce total

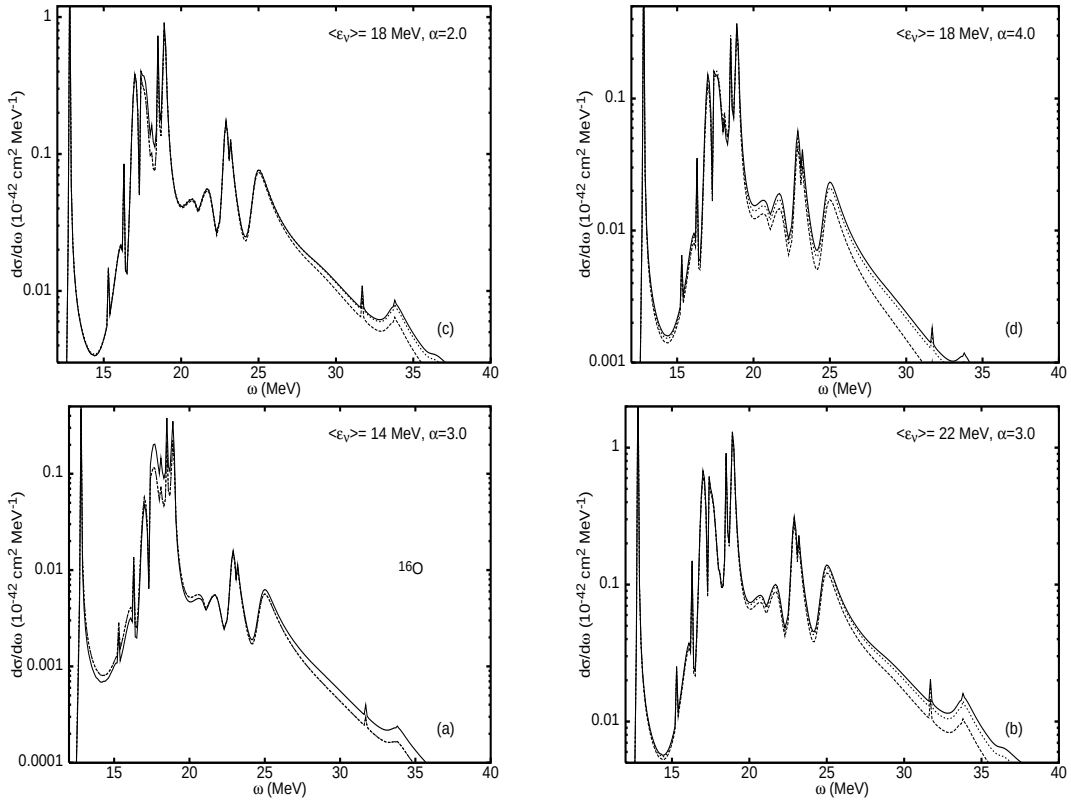

Figure 7: Comparison between differential cross sections for neutral-current scattering on ^{16}O, folded with a power-law supernova-neutrino spectrum (full line) and synthetic spectra with 3 (dashed line) and 5 components (dotted line) for different energy distributions : $\langle\varepsilon\rangle$=14, α=3 (a), $\langle\varepsilon\rangle$=22, α=3 (b), $\langle\varepsilon\rangle$=18, α=2 (c), and $\langle\varepsilon\rangle$=18, α=4 (d).

and differential folded supernova-neutrino cross-sections very accurately, as Fig.7 illustrates.

References

[1] P. Vogel, Prog. Part. Nucl. Phys. **48**, 29 (2002).

[2] G. M. Fuller, W. C. Haxton and G. C. McLaughlin, Phys. Rev. D **59**, 085005 (1999).

[3] J. Engel, G. C. McLaughlin and C. Volpe, Phys. Rev. D **67**, 013005 (2003).

[4] C.J. Clarence, the SNO Collaboration, Nucl. Phys. Proc. Suppl. **100**, 326 (2001).

[5] Y. Oyama *et al.*, Phys. Rev. Lett. 56, 2604 (1987).

[6] M. Aglietta, P. Antonioli, G. Bari, C. Castagnoli *et al.*, Nucl. Phys. Proc. Suppl. **138**, 115 (2005).

[7] M.K. Sharp, J.F. Beacom, J.A. Formaggio, Phys. Rev. D **66**, 013012 (2002).

[8] R.N. Boyd and A.St.J. Murphy, Nucl. Phys. **A688**, 386c (2001).

[9] C.K. Hargrove *et al.*, Astroparticle Physics **5**, 183 (1996).

[10] B.E. Bodmann *et al.*, Phys. Lett. **B 332**, 251 (1994).
[11] http://www.phy.ornl.gov/nusns
[12] K. Langanke, G. Martínez-Pinedo, B. Müller, H.-Th. Janka et al, Phys. Rev. Lett **100**, 011101 (2008).
[13] E. Kolbe, K. Langanke, S. Krewald and F.K. Thielemann, Nucl. Phys**A540**, 599 (1992).
[14] C. Volpe, N. Auerbach, G. Coló, T. Suzuki, N. Van Giai, Phys. Rev. C **62**, 015501 (2000).
[15] A. Samana, F. Krmpotić, N. Paar, C. Bertulani, Phys. Rev. C **83**, 024303 (2011).
[16] N. Jachowicz, K. Heyde, J.Ryckebusch, and S. Rombouts, Phys. Rev. C**59**,3246 (1999).
[17] N. Jachowicz, K. Heyde, J.Ryckebusch, and S. Rombouts, Phys. Rev. C**65**, 025501 (2002).
[18] N. Jachowicz, K. Heyde, and J. Ryckebusch, Phys. Rev. C **66**, 055501 (2002).
[19] M. Keil, G.G. Raffelt, H.-T. Janka, Astrophys. J. **590**, 971 (2003).
[20] N. Jachowicz, K. Heyde, Phys. Rev. C **68**, 055502 (2003).
[21] P. Zuchelli, Phys. Lett. **B532**, 166 (2002).
[22] C. Volpe, J. Phys. **G30**, 1 (2004).
[23] J. Serreau, C. Volpe, Phys. Rev. C **70**, 055502 (2004).
[24] G. C. McLaughlin, Phys. Rev. C **70**, 045804 (2004).
[25] http://beta-beam.web.cern.ch/beta-beam
[26] N. Jachowicz, G.C. McLaughlin, Phys. Rev. Lett. **96**, 172301 (2006).
[27] N. Jachowicz, G.C. McLaughlin, C. Volpe, Phys. Rev. **C77**, 055501 (2008).